S. Mader
A. E. Blakeslee

On Dislocations in $GaAs_{1-x}P_x$

Abstract: Misfit dislocations in epitaxially grown layers of $GaAs_{1-x}P_x$ with a lattice constant gradient are examined by transmission electron microscopy. In specimens with (113)A growth planes, they form a three-dimensional arrangement of glissile and sessile dislocations. Cross slip is an important process in the generation of the dislocations. High resolution microscopy shows 1) glissile dislocations dissociated into partial dislocations and 2) undissociated sessile Lomer dislocations. These differences are attributed to contributions to the dislocation core energy from wrong bonds and dangling bonds. Screw dislocations are also thought to be undissociated, which facilitates cross slip and multiplication of dislocations.

Introduction

Dislocations play important roles in semiconductor devices. When acting as misfit dislocations, they relieve epitaxial stresses and accommodate changes in lattice constants frequently associated with epitaxial crystal growth [1]. However, dislocations often have an adverse influence on device operation. For example, by acting as recombination centers they reduce the efficiency of light-emitting devices [2]. Dislocations can also accelerate aging and deterioration of devices by providing paths for enhanced diffusion [3]. It is therefore desirable to understand the mechanisms that control the generation and motion of dislocations in diamond-like crystal structures in order to be able to optimize their various influences. The behavior of dislocations in these structures is not as well established as in metals. The purpose of this paper is to present transmission electron microscope (TEM) observations on $GaAs_{1-x}P_x$ from which new insight can be gained into the structure and dynamics of dislocations in III-V compounds.

The work reported here deals with dislocations in chemically vapor deposited, graded heterojunctions of $GaAs_{1-x}P_x$ in which $0 < x < 0.3$ [4]. Previous work has shown that glide of dislocations takes place in and into those regions having lattice constant gradients [5, 6]. This mode of dislocation motion can be considered as a small plastic deformation resulting in stress relief within the originally coherent (i.e., elastically strained) epitaxial layer. After the stress has relaxed, the dislocations remaining in the graded region are predominantly of the same sign, consistent with their role as misfit dislocations. (For example, the extra half-plane is extended toward the growth surface if the lattice constant of the overgrowth is smaller than that of the substrate.) This constraint results in a somewhat different and simpler dislocation arrangement compared to that produced by bulk plastic deformation.

Stress-induced glide proceeds, of course, along crystallographic elements; in diamond-like structures, dislocations glide on {111} planes with $a/2$ ⟨110⟩ Burgers vectors, their motion being controlled by the shear stress components along these glide elements [7]. This property suggested an investigation of the variation of the dislocation arrangements with different growth plane orientations and different relative shear components for the various glide systems. In the (001) orientation, the one which has been most extensively investigated, the shear stresses acting on all four glide planes are equal.

In general, a dense, complex, three-dimensional network of interconnected dislocation lines was observed, which, as expected, differed according to growth-plane orientation. In the work described here, the (113)A orientation was used; that is, the crystal was grown on that side of the polar (113) plane which exposed a predominance of "A", or Ga, atoms, as opposed to "B," or Group V, atoms. With (113)A growth planes an arrangement was found that could be unraveled into its components and analyzed in more detail than most other networks. This analysis is the main topic of the present paper, although the conclusions with regard to dissociation into partial dislocations, cross slip, and formation of Lomer dislocations are important for all aspects of dislocations in $GaAs_{1-x}P_x$ and other III-V compounds.

We first review several concepts regarding dislocations in diamond-like structures. Experiments and observations are then described for the dislocation arrangement on the scale of a few micrometers (in the section entitled

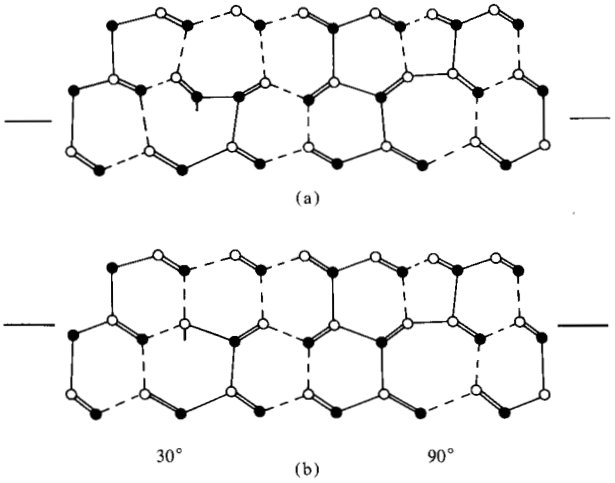

Figure 1 Dissociated 60° dislocations in the sphalerite structure with 30° and 90° partial dislocations and an intrinsic stacking fault lying between them. (a) Shuffle set; (b) glide set.

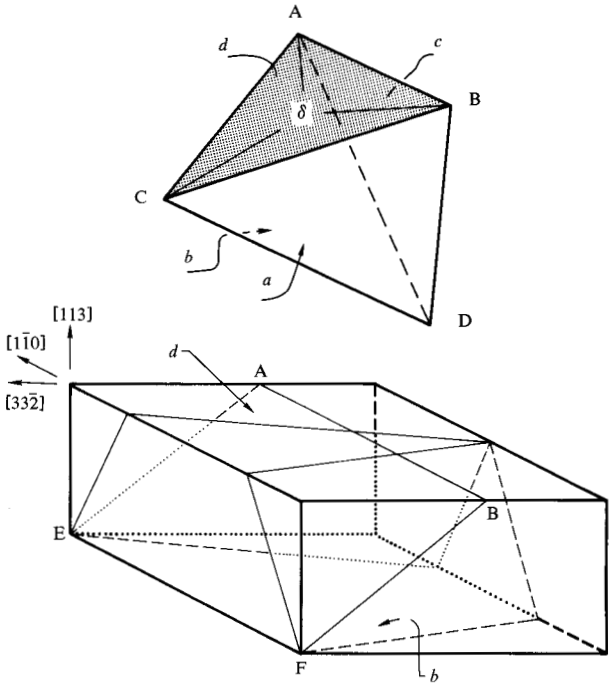

Figure 2 Perspective views of (a) Thompson tetrahedron of glide planes and Burgers vector directions and (b) {111} planes in (113)-oriented crystal.

"Dislocation arrangement"), and then on individual dislocations on the scale smaller than 100 Å (in the section entitled "Extended dislocations"). Conclusions are then drawn about the dislocation structure on an atomic scale.

Dislocations in the sphalerite structure

We briefly discuss certain aspects of dislocations which are unique to crystals having the sphalerite structure. Dislocations in diamond-like materials have been extensively reviewed by Alexander and Haasen [8, 9]. There are two open questions. The first one concerns the precise location of the glide plane. In crystals having the sphalerite (or diamond) structure, with lattice constant a, the {111} planes occur as double layers with a small internal spacing, $a/4\sqrt{3}$, and a larger external spacing, $3a/4\sqrt{3}$. Hirth and Lothe [7] pointed out that the glide plane of a dislocation can cut either through the small internal spacing or through the larger external spacing. The latter case is commonly assumed to be what actually takes place. The set of dislocations with the first configuration is called the glide set and the second one, the shuffle set. It is not clear from the literature which set participates in plastic flow [10].

The second open question concerns the possibility of dislocations dissociating into Shockley partial dislocations separated by a ribbon of stacking fault, a reaction that reduces the elastic energy of a dislocation line. Hornstra [11], Holt [12], and Hirth and Lothe [7] have discussed and illustrated the geometrically possible modes of dissociation. Figure 1 shows a dissociated 60° dislocation projected onto that {110} plane which is perpendicular to the line direction. Filled circles represent atoms of one element of the III-V compound, and open circles are atoms of the other element. Atoms connected by continuous lines are situated in the plane of the paper, and atoms connected by broken lines lie in superposed positions above and below the plane of the paper. The superposed atoms are connected to atoms in the plane of the paper by double lines. An intrinsic stacking fault exists on the middle plane of atoms between the two partial dislocations which lie in the regions labeled 30° and 90°, respectively. The top part of Fig. 1 shows the dissociation of a shuffle dislocation (more properly considered as an association of a perfect dislocation with a stacking fault on the next {111} plane [8]) and the bottom part that of a glide dislocation. It can be seen that at the 90° partials each atom is surrounded by four neighbors, although one of the bonds is a wrong one (being between identical nearest neighbors). At the 30° partials, the tetrahedral surrounding of one atom is violated, as shown by the dangling bond, and in the shuffle set there is also a wrong bond between nearest neighbors. Undissociated 60° dislocations of both sets (as well as any dislocation with an edge component) would have dangling bonds at the termination of the extra half-planes; in addition, those of the glide set would have wrong bonds between identical nearest neighbors. Other illustrations of possible core structures can be found in the literature [7, 10-12].

Although early TEM work indicated possible dissociation in diamond-like structures (cf. [10]), the experimental situation was not clear until recently, when extended dislocations were unambiguously observed by high resolution (weak-beam) TEM in Si [13] and Ge [10, 14] and as part of the present work in $GaAs_{0.7}P_{0.3}$ [15]. In general, the width of the stacking fault ribbon in an extended dislocation is determined by the equilibrium between elastic repulsion of the partial dislocations and the energy per unit area, γ, of the stacking fault. Stacking fault energies determined by using weak-beam TEM observations are: for Si, $\gamma = 5.5 \times 10^{-6}$ J/cm^2; and for $GaAs_{0.7}P_{0.3}$, $\gamma = 4.3 \times 10^{-6}$ J/cm^2. In close-packed metals with γ values in this range, all the dislocations dissociate in accord with the interplay between elastic repulsion and γ. However, this is not necessarily the case for crystals with the sphalerite structure. New influences arising from the core structure can oppose dissociation in certain cases. Hornstra [11] has shown that undissociated screw dislocations can take up a core arrangement in which each atom is tetrahedrally surrounded and no dangling bonds occur. Holt [12] drew attention to possible increases in energy associated with wrong bonds at partial dislocations. Perfect edge dislocations along ⟨110⟩ lines present an interesting case. They are sessile dislocations that can form as a result of reactions between glissile dislocations. According to Hornstra [11] they can exist without dangling bonds in both the unextended (Lomer) and extended (Lomer-Cottrell) configurations, although the number of wrong bonds is different for the two configurations. We will discuss the case in more detail in the section on extended dislocations.

A third aspect of dislocations in crystals with the sphalerite structure arises from the polarity of the {111} glide planes. If the filled circles in Fig. 1 represent atoms of Group III elements and the open circles atoms of Group V elements, the figure shows α-dislocations; with filled and open reversed it corresponds to β-dislocations. The mobility of α-dislocations is known to be somewhat higher than that of β-dislocations [8, 16]. The present paper deals only with observations on (113)A growth planes and cannot distinguish possible differences between the two types. But we note that dislocations on glide planes *a* and *b* of Fig. 2 are α-dislocations and those on plane *d* are β-dislocations.

Experimental procedures

$GaAs_{1-x}P_x$ specimens were prepared by a standard method of chemical vapor deposition, namely the AsH_3-PH_3-Ga-HCl-H_2 vapor epitaxial process [17]. Chemically and mechanically polished GaAs substrates oriented in the [113]A direction were used. The substrate temperatures were between 750 and 790 °C. A few micrometers of GaAs were first grown. Then the PH_3 was introduced through a programmed flow controller to increase the value of x from 0 to 0.38 in a nearly linear fashion over a distance of typically 12 μm. The phosphorus gradient was thus about 3%/μm, which corresponds to a gradient of the lattice constant of $1/a \cdot da/dz = 11/\text{cm}$ [6]. TEM foils were prepared by first etching back from the growth surface to a composition of about $GaAs_{0.7}P_{0.3}$ and then jet etching a dimple on the substrate side with a solution of 15 drops of Br_2 in 100 ml of CH_3OH.

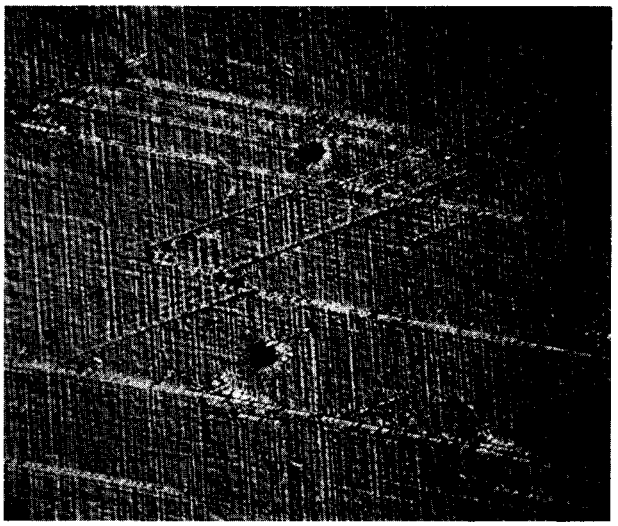

Figure 3 Optical micrograph of (113)A etched growth surface, showing how {111} planes intersect growth plane along three directions. ×140.

Figure 2 shows the disposition of the {111} planes in a crystal having a (113) growth plane, together with a Thompson tetrahedron of glide planes and Burgers vector directions, labeled in the usual way [7]. Both parts of the figure are drawn as viewed in the same perspective projection. The {111} planes intersect the growth plane along three directions, forming an isosceles triangle. An optical micrograph, Fig. 3, of the etched growth surface clearly shows these three directions. Large areas are homogeneously covered with traces of plane *d*. It is in those areas that the dislocation arrangement was analyzed. Briefly, it arose from predominance of glide on plane *d*, which relieves misfit mainly in the direction $[33\bar{2}]$ of Fig. 2. Other areas of Fig. 3 show strong traces of planes *a* and *b*. Here the dislocation arrangement was too complex for TEM analysis. However, x-ray topography indicated large amounts of shear on planes *a* and *b* in these areas; this relieves misfit mainly in the direction $[1\bar{1}0]$.

Stereo TEM micrographs were obtained by tilting the TEM foils about the direction AB. Stereoscopy proved to be very valuable for the analysis of three-dimensional dislocation arrangements. The micrographs of the next

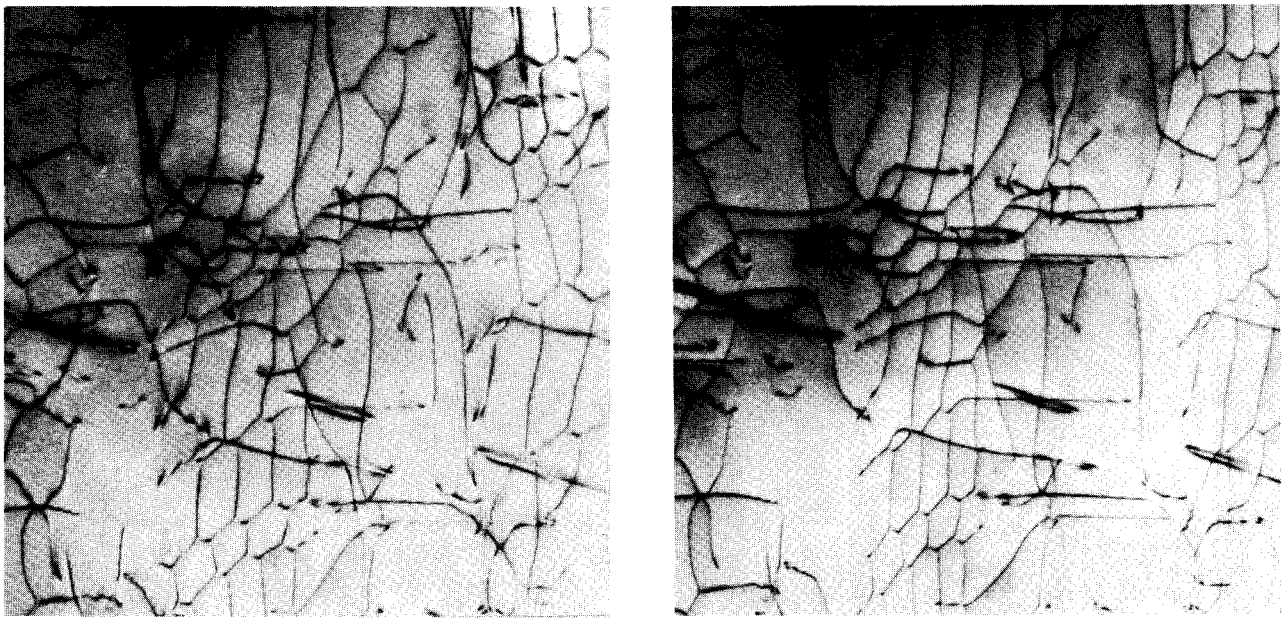

Figure 4 Stereo transmission electron-microscope pair showing networks of elongated dislocation cells (see text). $g = [2\bar{2}0]$. ×30 000.

section are oriented as indicated in Fig. 2, namely plane *d* extends from the lower left (EF) to the upper right (AB). The TEM observations and their discussions are divided into two parts: the overall dislocation arrangement in thick (up to 5 000 Å) portions of the foils and the high resolution observation of selected features in thin portions of the foil. The weak-beam methods used in the second part have already been described [15].

Dislocation arrangement

• *Observations*

Figure 4 is a stereo pair of a typical section. The most striking features are networks of elongated dislocation cells located on planes of type *d*. Individual network planes are separated by about one μm. The networks consist of a set of dislocations, about 0.2 μm apart, running from top to bottom in Fig. 4 with Burgers vectors corresponding to CB in Fig. 2. They are cross-linked by dislocations with Burgers vectors AC and BA (Fig. 2). The assignment of Burgers vectors can be verified with the aid of Fig. 5, where the same area is shown with various diffracting conditions. Each diffracting condition extinguishes the contrast of dislocations having one set of Burgers vectors. The average direction of the cross links is frequently close to direction AC. A schematic drawing illustrating this linkage is at the center of Fig. 8. The remainder of Fig. 8 is discussed in the next section.

The network planes are interconnected by dislocations on plane *b* with Burgers vectors AC and by very straight dislocations with line directions CD and Burgers vectors BA. The latter ones are perfect edge dislocations and they are not glissile. (Their glide plane would be the unfavorable (001) plane). We will refer to the BA dislocations in this orientation as Lomer dislocations. This implies that we consider them as arising from reactions of dislocations with Burgers vectors CB and AC. Examples of terminations of Lomer dislocations at three-fold nodes with BA → CB+ AC can indeed be found in Fig. 4. Another example is marked in Fig. 6, which is the area adjoining Fig. 4 on the left. (Markings on stereo pairs interfere with the visual three-dimensional effect.) The dislocation labeled BA has the straight Lomer orientation to almost the bottom of the foil, then turns onto plane *d*, where it continues for about 0.2 μm in direction CA, and subsequently splits into two dislocations having Burgers vectors CB and AC.

It is interesting to note that all the Burgers vectors are parallel to plane *d*. Dislocation lines located on plane *b* can, therefore, cross slip into plane *d*. In Fig. 4, examples can be found where dislocations with Burgers vector AC change their glide plane from *b* to *d*; one such case is also marked in Fig. 6.

In foils that were not back-etched and showed the arrangement close to the growth surface, only one set of dislocations was observed in significant numbers. This set was located on particular planes of type *d* and had no cross links. This shows that the formation of networks is a secondary event. Also present near the growth surface were occasional Lomer dislocations. Further deductions based on these foils cannot be justified, because observations just below the unetched growth surface do not

(a)

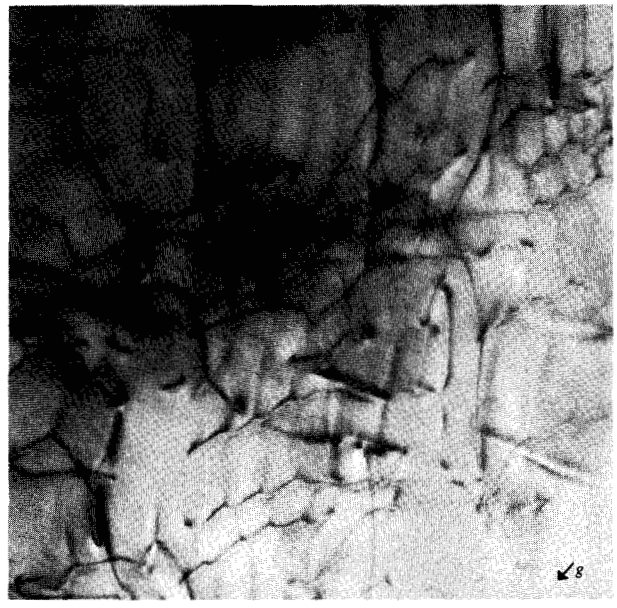

(b)

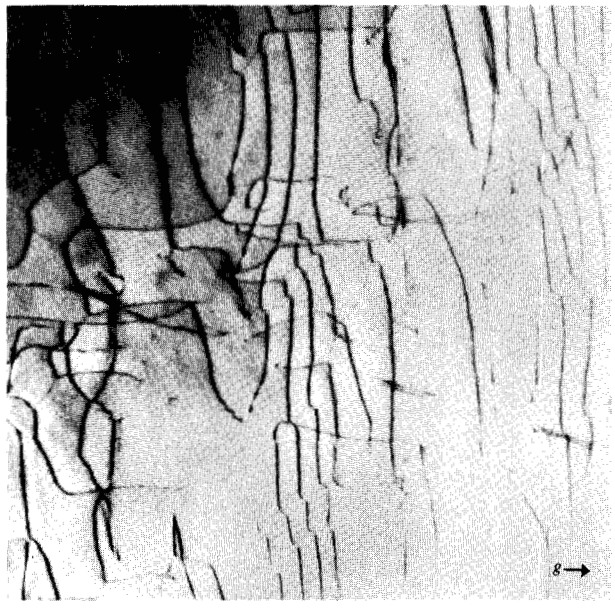

(c)

Figure 5 TEM micrographs of same area as Figure 4, with different diffracting conditions. (a) $g = [3\bar{1}\bar{1}]$, extinguishing AC (b) $g = [\bar{1}3\bar{1}]$, extinguishing CB, (c) $g = [\bar{2}\bar{2}0]$, extinguishing BA.

truly represent the dislocation arrangement in steady state growth conditions. This is so because after the vapor supplies are shut off, and while the specimens are cooling down, they still receive a deposit of about 0.5 μm, which changes the epitaxial strain pattern in a temperature range where the dislocations are just becoming immobile.

The directions AC and CB are symmetrical with respect to the $[33\bar{2}]$ direction in Fig. 2. Correspondingly, the roles of Burgers vectors AC and CB in the networks were found to be interchanged in other areas of the foil. There the long segments have Burgers vector AC and the cross links have CB. Regions of one or the other type extend typically about 5 to 10 μm.

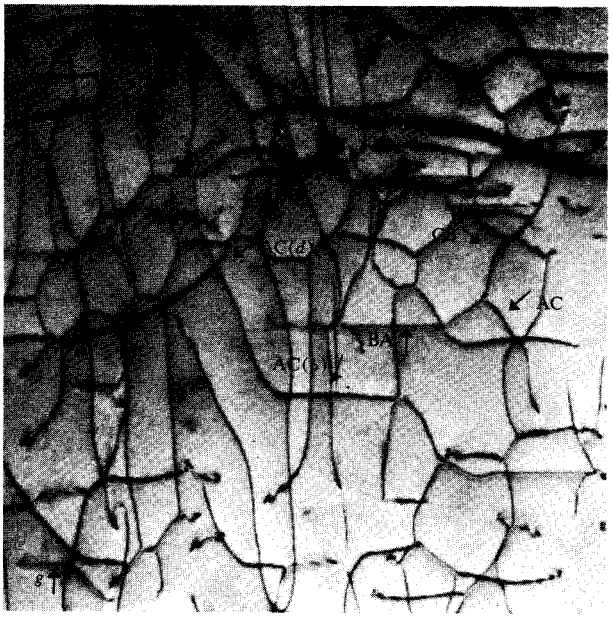

Figure 6 TEM micrograph, adjoining Fig. 4. ×30 000.

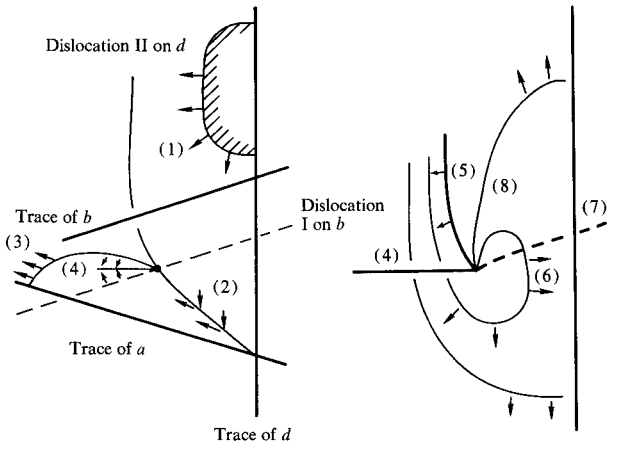

Figure 7 Proposed mechanism for formation of a Lomer dislocation and of a dislocation source.

• *Discussion*

We now show how the arrangement can be generated from a sequence of plausible events. We have to postulate that 1) a few dislocations with Burgers vectors AC and CB exist or can be nucleated; 2) cross slip occurs easily; and 3) intersection [18] of dislocations is difficult, i.e., there is a considerable "forest hardening." In face-centered cubic metal crystals both cross slip and intersection occur either easily, if the stacking fault energy γ is high, or with difficulty, if it is low and the dislocations are dissociated. Dislocation interactions and hardening mechanisms in the bulk form of these materials are reviewed, for example, in Refs. [19], [20], and [21]. In epitaxial films, however, dislocations can behave differently. For example in films of gold, a typical low-γ material, Matthews observed frequent cross slip [22].

The observations suggest strongly that the first step in the formation of networks is the introduction of the long dislocation segments with Burgers vector CB, which we shall call primary dislocations. Considerable numbers of primary dislocations are always located on individual planes d, forming a pileup in the lattice constant gradient. This implies their origin from one common source or multiplication event. For this event, we propose the mechanism illustrated in Fig. 7. The left-hand part of the figure shows the view onto the growth plane (see Fig. 2) with traces of planes a, b, and d. A dislocation (I) with Burgers vector AC exists on plane b below the surface (broken line). Another dislocation half-loop (II) with Burgers vector CB is located on plane d and spreads down from the growth surface under the influence of the stress associated with the lattice constant gradient as indicated by arrows (1). Upon meeting and not intersecting dislocation I, an appreciable length of dislocation II is pulled into screw orientation (2), cross slips onto plane a, and continues to glide to the left (3). Along some distance to the left of the point of impaction both dislocations can combine to form a Lomer dislocation with Burgers vector BA (4). The resulting configuration is shown with heavy lines at the right of Fig. 7. It represents a Frank-Read source operating near a free surface. The Lomer dislocation is not glissile and provides an anchor point for segment (5) of dislocation II. This segment continues to move and multiply and to generate a pileup of primary dislocations on plane d below the anchor point.

Configurations at various stages of this sequence [except for the dislocation segment in reverse orientation (6)] can be found in the micrographs. Such a segment would, of course, be very strongly attracted to the free surface and would not survive in the completed dislocation arrangement. Segment (7) of the original dislocation I can also cross slip onto plane d and react with segment (8) of a primary dislocation. This configuration is pointed out in Fig. 6.

We now turn to the weaving of cross links in the network. In Fig. 8 at the top, a dislocation half-loop located on plane b and having a Burgers vector AC expands (1) and meets a primary dislocation pileup located on plane d. Instead of intersecting the primary dislocations it is also pulled into screw orientation over the whole width of the primary pileup (2). Upon cross slipping onto plane d the dislocations can now react first to form short segments with Burgers vector BA (3), and then this configuration can relax into cross links with sections of approximately equal length (4). The section of the original dislocation that is not impeded by the pileup can ei-

ther continue to glide on plane b (5) or it can combine with the last dislocation of the pileup to form a Lomer dislocation (6).

Similar reactions can be constructed when the type I and type II dislocations meet in other configurations. As a result, the volume of graded material is filled with an arrangement of dislocations with extra half-planes extending to the free surface and thus serving to accommodate the lattice constant gradient. The dislocations can cross slip between planes a and d through the common Burgers vector CB and likewise between planes b and d through AC. There is also a large number of Lomer dislocations. It is interesting to note that these dislocations are not the ones experiencing the highest shear stress, τ, in a system with (113) growth plane geometry. For dislocations on plane b, the ratio τ/σ (where σ is the biaxial normal stress parallel to the growth plane) is 0.223 for Burgers vector AC, whereas it is 0.445 for Burgers vector AD, and one would therefore expect dislocations of the latter type to be nucleated more frequently than those of the former one. They were, however, not present in the networks. Even though they may have been nucleated or propagated out of the substrate, dislocations with Burgers vector AD did not contribute to the buildup of the three-dimensional arrangement. In order for them to do so, a similar spreading mechanism involving cross slip onto plane c and formation there of a source similar to that shown in Fig. 7 would be necessary. However, for such a source the resolved shear stress is quite low ($\tau/\sigma = 0.148$), and a resulting dislocation on plane c accommodates very little misfit because the projection in the growth plane of the edge component of its Burgers vector AD is very small.

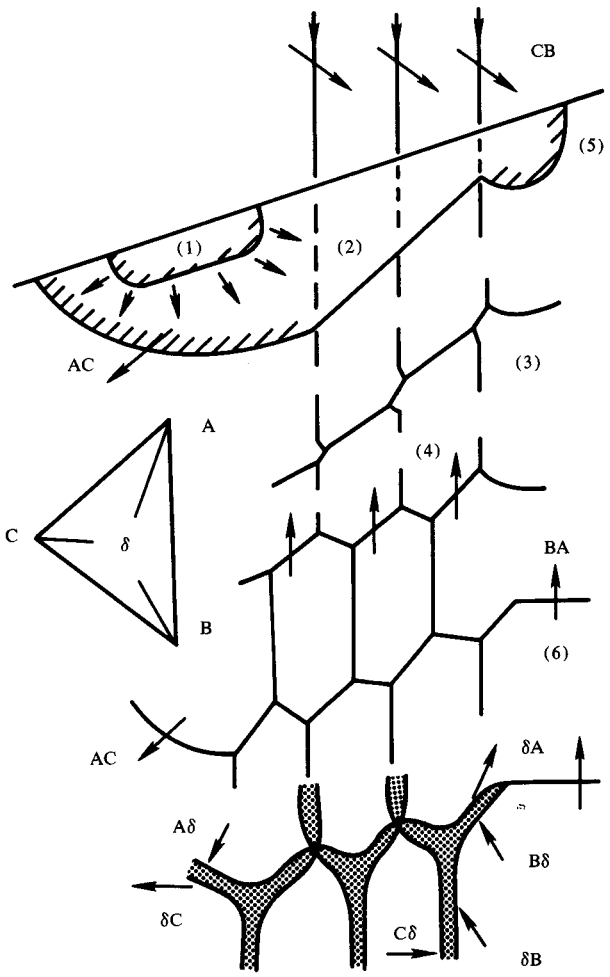

Figure 8 Formation of cross-links between a pileup of primary dislocations.

Extended dislocations

• *Observations*

We now describe high resolution TEM observations of dissociated dislocations. Figures 9(a) and 9(b) show weak-beam, dark-field micrographs of one cell of a network on plane d, together with a Lomer dislocation which forms the connection to another network plane. The dislocations on planes d are extended and in the network cell they form alternately extended and contracted nodes. In Fig. 9(a), where some of the dislocations are labeled in accordance with the bottom section of Fig. 8 and where the diffraction vector is $[\bar{1}\bar{1}1]$ (normal to plane c), the fringe contrast of the stacking faults is prominent. In Fig. 9(b), with diffraction vector $[2\bar{2}0]$ (parallel to AB), only dislocation contrast is visible. Partial dislocations with Burgers vector Cδ are invisible, as expected [13].

Widths of the extended dislocations and dimensions of the stacking fault nodes have been measured and the stacking fault energy evaluated, using the usual concept of an equilibrium configuration in which the elastic interaction of the partials is balanced against the specific surface energy, γ, of the stacking fault [23]. The result was $\gamma/Gb = 3.75 \times 10^{-3} \pm 15\%$, where $G = 0.51 \times 10^{12}$ dyn/cm^2 is the shear modulus and $b = 2.25$ Å is the magnitude of the Burgers vector of partial dislocations in $GaAs_{0.7}P_{0.3}$; or $\gamma = 4.3 \times 10^{-6}$ J/cm^2 [15].

There is another noteworthy feature in Fig. 9. The Lomer dislocation with Burgers vector BA and line direction CD is one of those dislocations mentioned in the second section in which the core structure possibly prevents dissociation. This dislocation is visible in Fig. 9(b) but invisible in Fig. 9(a), where the diffraction vector is perpendicular to BA. Dissociated dislocations (on plane d) with the same total Burgers vector are, however, clearly visible in Fig. 9(a). This indicates that, when the dislocation has the Lomer orientation, dissociation does not take place.

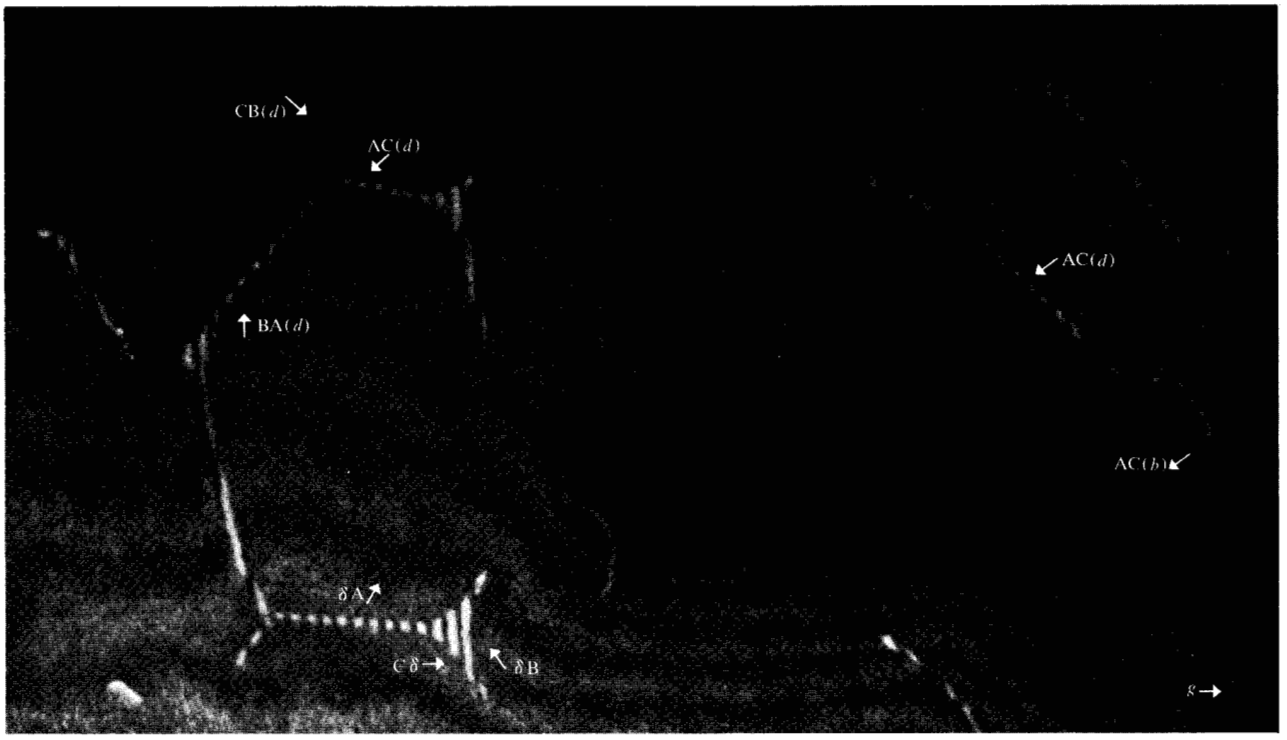

(a)

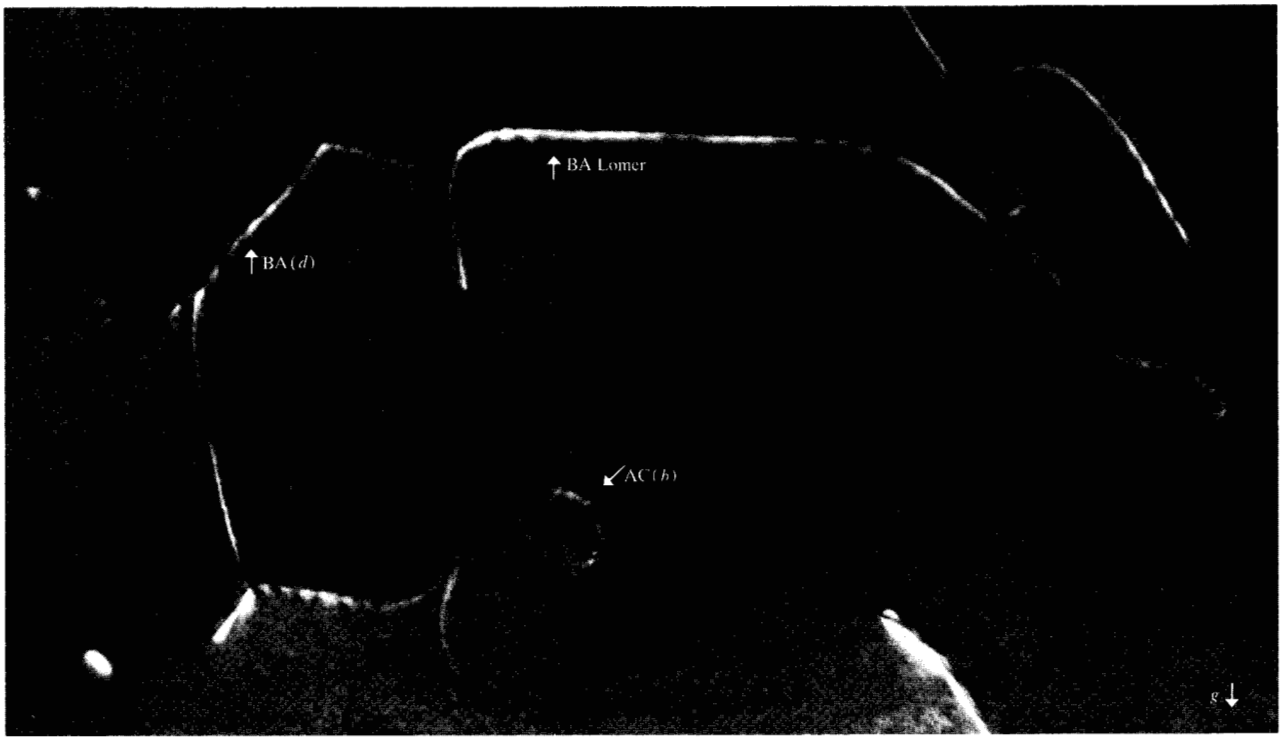

(b)

Figure 9 Weak-beam, dark-field micrographs showing dissociated dislocations. ×165 000. (a) $g = [\bar{1}\bar{1}1]$ with $6g$ strongly excited. (b) $g = [\bar{2}20]$ with $3g$ strongly excited.

Based on the usual balance between elastic repulsion and stacking fault energy γ, the Lomer dislocation with Burgers vector BA would be expected to dissociate into a Lomer-Cottrell dislocation with two 90° partials on planes a and b and another partial along the original line direction. The latter partial is connected to the other two by stacking fault ribbons on planes a and b, respectively. The question is now whether these ribbons would be visible in Fig. 9(a). We estimate their widths by extrapolating width calculations for metals with similar γ/Gb values (silver) [24] and expect a dissociation of about 50 Å. Such a ribbon should be visible in Fig. 9(a) since stacking fault contrast of other dissociated dislocations on plane b is clearly visible. A deliberate search using a variety of other imaging conditions revealed no evidence for dissociation of any Lomer dislocation.

The other case mentioned in the second section with possible influence of the core on dissociation is a dislocation in screw orientation. Unfortunately, a search for screw dislocations was fruitless; not a single segment in perfect screw orientation was observed in the completed dislocation networks. But many dislocations were observed with line segments on two different glide planes. If a dislocation glides from one plane to another, it can do so only by cross slip of a segment in screw orientation. Therefore, during the formation of the dislocation networks an appreciable number of segments must have been momentarily in screw orientation and, as such, they cross slipped easily.

An example of a dislocation with segments on two planes can be seen in Fig. 9. At the right a dislocation with Burgers vector AC is located on plane d and further to the right it continues on plane b, as can be seen from the stacking fault fringes. Close to the intersection of the two planes the dislocation has moved away from pure screw orientation towards an edge orientation on both glide planes. The dissociation appears to be reduced near the intersection. This situation was observed only once, however, and will not be discussed further.

• *Discussion*

Weak-beam TEM micrographs show that glissile dislocations with an edge component dissociate into partial dislocations separated by a stacking fault. It is difficult for these dislocations to intersect one another, and one of the postulates in the section entitled "Dislocation arrangement" follows now as a natural consequence. Before intersection can take place, the partials have to be pushed together into a constricted configuration [19]. This will become less and less possible with increasing relief of epitaxial stress.

The value of the stacking fault energy, γ, 4.3×10^{-6} J/cm^2 for $GaAs_{0.7}P_{0.3}$, is in the range of values for other diamond-like crystals (which extends from 6.9×10^{-6} J/cm^2 for Ge to 2×10^{-6} J/cm^2 for InAs) [10]. But an interesting difference exists between Si and $GaAs_{1-x}P_x$ with regard to the nature of the stacking fault. In Si extended nodes with alternate intrinsic and extrinsic stacking faults have been observed [13], whereas in the present material, extended and contracted nodes with only intrinsic faults were found. Dissociation of 60° dislocations does occur, therefore, according to Fig. 1(a) or Fig. 1(b) (we return later to the case of screw dislocations) and the wrong bond at the 90° partial does not prevent dissociation in this case.

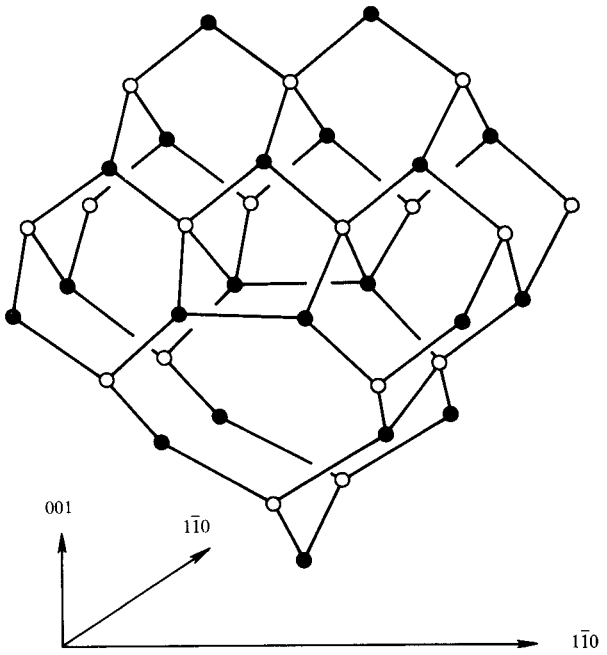

Figure 10 Model of the core of a Lomer dislocation in the sphalerite structure with Burgers vector $a/2$ [1$\bar{1}$0] and line direction [$\bar{1}$10].

Weak-beam TEM micrographs also show that Lomer dislocations are undissociated. Figure 10 shows a perspective view of the core of a Lomer dislocation (after Hornstra [11], adapted to the sphalerite structure) formed by combining two 60° dislocations (with Burgers vectors $a/2$ [$\bar{1}$01] on (11$\bar{1}$) and $a/2$ [01$\bar{1}$] on (111)) of the shuffle set. It can be seen that each atom is surrounded by four nearest neighbors, so there are no dangling bonds. Similarly to the 90° partials in Fig. 1, there is a wrong bonding sequence between two rows of atoms, each having one identical nearest neighbor. Figure 11(a) shows the projection of the same core structure onto the (110) plane, again for the shuffle set. Hornstra has shown for the diamond structure that this dislocation can dissociate into a Lomer-Cottrell one without violating the tetrahedral surrounding of any atom. This is, of course, also true in the sphalerite struc-

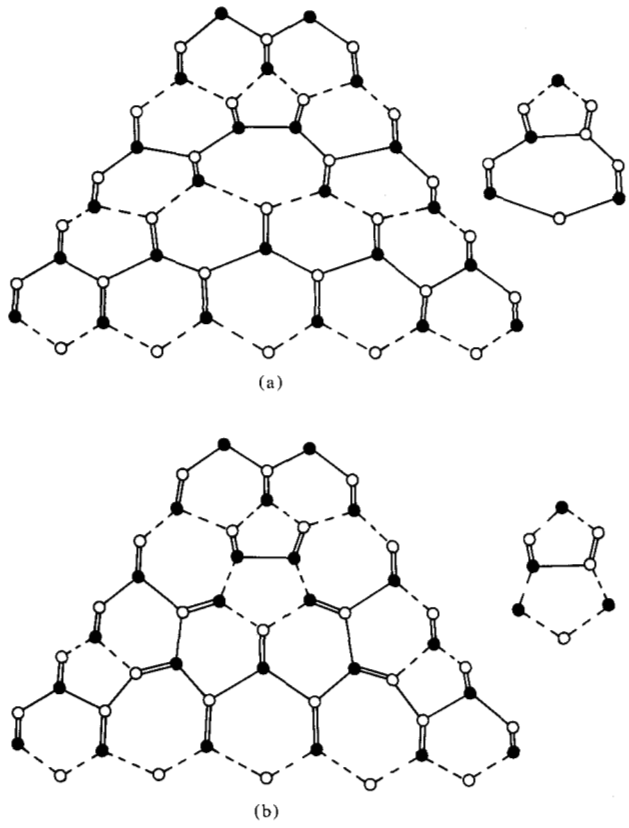

Figure 11 *One mode of dissociation of a Lomer dislocation.* a) Projection of a Lomer dislocation along the line direction. b) Projection showing dissociation into a Lomer-Cottrell dislocation along the line direction. The number of wrong nearest-neighbor bonds increases considerably.

ture; however, the number of wrong nearest neighbor bonds increases considerably. This can be seen in Fig. 1(b). There are rows of wrong bonds between identical neighbors in each of the 90° partials, and along the line of the original Lomer dislocation—i.e., along the so-called $\alpha\beta$ partial, using the notation of Thompson [7]—there are three rows of wrong bonds. It appears that the disadvantage of increasing the number of wrong bonds from one to five now overbalances the advantage to be gained by dissociation into partial dislocations.

If, however, the Lomer dislocation results from the combination of two 60° dislocations of the glide set, the disadvantage associated with wrong bonds in the dissociated configuration is less severe. At the right side of Fig. 11 the cores of the Lomer dislocations and of the $\alpha\beta$ partial are redrawn for the glide set, and it can be seen that in the core region the number of wrong bonds (three) does not change. The total number of wrong bonds in the dissociated configuration increases only by the two present at the 90° partials. Wrong bonds at 90° partials are not an obstacle to dissociation; this is clear from the behavior of 60° dislocations (Fig. 1). One might therefore expect the Lomer dislocation to be extended into the Lomer-Cottrell configuration, if glissile dislocations should belong to the glide set. We consider the observation of the opposite behavior as an indication that the dislocations actually belong to the shuffle set, as drawn at the top of Fig. 1.

Counting the number of wrong bonds is, of course, a very crude measure of the extra core energy associated with partial dislocations. It is not yet clear whether this energy has the character only of a Madelung energy arising from rows of atoms residing in the wrong sublattice or whether it also has a contribution which depends strongly on the relative position of the rows. In the first case the extra energy would act as a barrier to dissociation and, once the barrier is overcome, the equilibrium configuration would be determined in the usual way by stacking fault energy and elastic energy only. In the second case, the extra energy would also cause an extra force between partial dislocations. This extra force would enter into the equilibrium configuration and would necessitate a correction in the determination of the stacking fault energy. Further calculations and observations on a variety of III-V compounds with different energies of wrong bonds will presumably clarify the picture. In the meantime, we emphasize that the core structure of partial dislocations can modify the configuration of extended dislocations and should be taken into account in addition to the elastic interactions and the stacking fault energy.

We were not able to observe a pure screw dislocation; thus we have no direct evidence whether one is dissociated or undissociated. The dissociated configuration of a screw dislocation is a stacking fault ribbon bonded by two 30° partials. Each of them contains an atom with a dangling bond and, in the case of the shuffle set, a wrong bond between identical neighbors (see Fig. 1). Following arguments by Hornstra [11] and Holt [12] and extending our above reasoning, we expect a screw dislocation to be undissociated.

Cross slip of extended screw dislocations is not a simple process, and, for example, in fcc metal crystals, it occurs only at high stress levels [20]. The extended ribbon has to be constricted over a short length and then has to dissociate again on the cross slip plane [19]. But these complications are absent for cross slip of undissociated screw dislocations, and in that case cross slip should occur easily. Frequent cross slip was also observed in slightly deformed silicon [25], where it plays a role in spreading slip and multiplying dislocations. Cross slip played a similar role in our discussion of the formation of the overall arrangement of misfit dislocations. We conclude that in both cases cross slip is facilitated by the

fact that the screw dislocations are not dissociated. Another one of the postulates in the section entitled "Dislocation arrangement" is now a natural consequence of the atomistic structure of the dislocation core.

Summary and conclusions

We have examined the three-dimensional arrangement of dislocations in epitaxial $GaAs_{1-x}P_x$ layers which have a gradient of lattice constant and phosphorus concentration. The elastic stress associated with the lattice constant gradient is the driving force which moves the dislocations into their positions. After achieving a small plastic strain and relieving the stress, the dislocations act as misfit dislocations and accommodate the change of lattice constant in the graded region.

The dislocation structure in large regions of crystal with (113)A growth planes was particularly suitable for analysis. We were able to show how the three-dimensional network can develop from a few seed dislocations and can propagate itself into the graded volume as long as the dislocations obey two rules: that intersection of glide dislocations be difficult and that cross slip occur easily.

Viewed from the large background of dislocation dynamics in face-centered cubic crystals, these two rules appear to be incompatible with each other. Dislocations are either unextended line defects that intersect and cross slip easily or they are extended, in which case both processes become more difficult the wider the stacking fault ribbon of the dislocations. But in the sphalerite structure both rules can be obeyed at the same time because not all types of dislocations are equally extended. Some configurations are prevented from dissociation because this would lead to broken bonds and to wrong bonds between identical nearest neighbors. We have shown that glide dislocations with an edge component are extended and therefore intersect with difficulty, and we have presented arguments that screw dislocations should be undissociated and cross slip readily. With these characteristics—which are derived from the dislocation core structure—one can proceed to build up the network of misfit dislocations.

We have also discussed another configuration, which could be unextended or extended, namely Lomer versus Lomer-Cottrell dislocations. We have shown that for one particular mode of dissociation the number of wrong bonds would increase from one to five. (Similar arguments can be made for other less probable modes of dissociation, which were discussed by Hirth [24]. The observations show that the unextended configurations are present, which lends weight to our hypothesis of the importance of the core structure. Lomer dislocations also played a role in our mechanism of dislocation multiplication.

In this paper we attempt to go beyond a mere description of the arrangement of dislocations and of pair-wise interactions, and we try to account for the generation of the whole dislocation structure as it occurs during crystal growth. This is possible because in (113)-oriented crystals the various different {111} planes play distinctly different roles. In the more extensively investigated [4, 6] and technologically more important (001) crystals, this distinction among the various {111} planes is lost. They all play the same roles both as principal slip planes and as planes which catalyze multiplication by cross slip. However, in retrospect, many features described for dislocations in (001) crystals [4, 6] can be identified with processes described here. Examples are Lomer dislocations, numerous nodes where intersection has been difficult, and segments of reacted dislocations which were formed with the same topology as discussed in connection with Fig. 8.

For practical applications, the graded region is followed by growth of a layer of the solid solution crystal having a constant composition, and here dislocations are undesirable. But dislocations cannot end inside a single crystal, and portions of the dislocations in the graded region are propagated as threading dislocations into the constant composition layer. Their density must be inversely proportional to the average mesh size of the network in the graded regions. In this connection, the formation of reacted segments leading to closely interconnected three-dimensional networks is unfortunate. The mesh size can, of course, be increased and the density of threading dislocations decreased by decreasing the gradient, as is well known to those who grow such crystals [4].

Acknowledgments

We are grateful for many helpful discussions with J. W. Matthews and for the assistance of B. K. Bischoff and A. Gilgore in the fabrication of specimens.

References and note

1. J. W. Matthews, *Epitaxial Growth*, Academic Press, New York, 1975.
2. A. H. Herzog, D. L. Keune, and M. Craford, *J. Appl. Phys.* **43,** 600 (1972).
3. P. M. Petroff and R. L. Hartman, *Appl. Phys. Letters* **23,** 469 (1973).
4. M. S. Abrahams, L. R. Weisberg, C. J. Buiocchi, and J. Blanc, *J. Mat. Sci.* **4,** 232 (1969).
5. M. S. Abrahams, J. Blanc, and C. J. Buiocchi, *Appl. Phys. Letters* **21,** 185 (1972).
6. S. Mader, A. E. Blakeslee, and J. Angilello, *J. Appl. Phys.* **45,** 4730 (1974).
7. J. P. Hirth and J. Lothe, *Theory of Dislocations*, McGraw-Hill Book Co., Inc, New York, 1968.
8. H. Alexander and P. Haasen, *Solid State Physics* **22,** 27 (1968).
9. H. Alexander and P. Haasen, *Annual Review of Materials Science* **2,** 291 (1972).

10. R. Meingast and H. Alexander, *Phys. Stat. Sol.* (A) **17,** 229 (1973).
11. J. Hornstra, *J. Phys. Chem. Solids* **5,** 129 (1958).
12. D. B. Holt, *J. Phys. Chem. Solids* **23,** 1353 (1962).
13. I. L. F. Ray and D. J. H. Cockayne, *Proc. Roy. Soc. Lond.* A **325,** 543 (1971).
14. F. Haeussermann and H. Schaumberg, *Phil. Mag.* **27,** 745 (1972).
15. S. Mader and A. E. Blakeslee, *Appl. Phys. Letters* **25,** 365 (1974).
16. S. A. Erofeeva and Yu. A. Osip'yan, *Sov. Phys. Solid State* **15,** 538 (1973).
17. J. W. Burd, *Trans. Met. Soc. AIME* **245,** 571 (1969).
18. The term "intersection" as applied to dislocations in this paper has the specialized connotation that the dislocations can easily pass through one another.
19. A. Seeger, in *Dislocations and Mechanical Properties in Crystals*, Eds. J. Fisher et al., John Wiley & Sons, Inc., New York, 1957, p. 243.
20. A. Seeger, S. Mader, and H. Kronmueller, in *Electron Microscopy and Strength of Crystals*, Eds., G. Thomas and J. Washburn, John Wiley & Sons, Inc., New York, 1963, p. 665.
21. F. R. N. Nabarro, Z. S. Basiuski, and D. B. Holt, *Adv. in Physics* **13,** 193 (1964).
22. J. W. Matthews, *Phil. Mag.* **13,** 1207 (1966).
23. L. M. Brown, *Phil. Mag.* **10,** 441 (1964).
24. Hirth and Lothe, *op. cit.*, p. 726.
25. Yu. V. Malov and V. N. Rozhanskii, *Sov. Phys.—Solid State* **9,** 805 (1967).

Received September 11, 1974

The authors are located at the Thomas J. Watson Research Center, Yorktown Heights, New York 10598.